HHS Public Access

Author manuscript

Biofabrication. Author manuscript; available in PMC 2015 June 01.

Published in final edited form as:

Biofabrication. 2014 June ; 6(2): 024111. doi:10.1088/1758-5082/6/2/024111.

3D Printing Facilitated Scaffold-free Tissue Unit Fabrication

Yu Tan[1,2], **Dylan J. Richards**[1,2], **Thomas C. Trusk**[2], **Richard P. Visconti**[2], **Michael J. Yost**[2], **Mark S. Kindy**[3], **Christopher J. Drake**[2], **William Scott Argraves**[2], **Roger R. Markwald**[2], and **Ying Mei**[*,1,2]

[1]Department of Bioengineering, Clemson University, Clemson, SC, USA

[2]Department of Regenerative Medicine and Cell Biology, Medical University of South Carolina, Charleston, SC, USA

[3]Department of Neurosciences, Medical University of South Carolina, Charleston, SC, USA

Abstract

Tissue spheroids hold great potential in tissue engineering as building blocks to assemble into functional tissues. To date, agarose molds have been extensively used to facilitate fusion process of tissue spheroids. As a molding material, agarose typically requires low temperature plates for gelation and/or heated dispenser units. Here, we proposed and developed an alginate-based, direct 3D mold-printing technology: 3D printing micro-droplets of alginate solution into biocompatible, bio-inert alginate hydrogel molds for the fabrication of scaffold-free tissue engineering constructs. Specifically, we developed a 3D printing technology to deposit micro-droplets of alginate solution on calcium containing substrates in a layer-by-layer fashion to prepare ring-shaped 3D hydrogel molds. Tissue spheroids composed of 50% endothelial cells and 50% smooth muscle cells were robotically placed into the 3D printed alginate molds using a 3D printer, and were found to rapidly fuse into toroid-shaped tissue units. Histological and immunofluorescence analysis indicated that the cells secreted collagen type I playing a critical role in promoting cell-cell adhesion, tissue formation and maturation.

Introduction

Tissue engineering holds remarkable promise for providing architecturally and functionally competent replacements for tissues damaged by injury, disease and aging [1-7]. During the last decades, both scaffold and scaffold-free tissue engineering strategies have been explored [8-13]. As the central portion of scaffold-based tissue engineering, biomaterials can provide molecular and mechanical signals to promote cell adhesion and proliferation, and enhance extracellular matrix (i.e., ECM) protein deposition and tissue formation [14, 15]. Although it retains a high potential for application, the scaffold-based approach faces numerous challenges. One of the key problems is that the ideal material to satisfy all the requirements for tissue engineering applications remains elusive. In addition, scaffold materials and their degradation products can introduce a variety of adverse effects [16]. As an alternative, bioprinting-based, scaffold-free tissue fabrication methods (i.e., organ printing) have been

[*]mei@clemson.edu.

explored [3, 16]. For example, Cyrille Norotte and coworkers developed a 3D printing technology to fabricate scaffold-free, vascular tissue engineered constructs [17]. This approach has several distinct advantages. In particular, it can allow for the creation of tissues with a high cell density. In addition, it can facilitate rapid tissue formation and accelerate tissue maturation [16, 17].

One core concept of organ printing is the use of tissue spheroids as building blocks to assemble functional tissues [3, 16]. Tissue spheroids are sphere-shaped micro-tissues formed by spontaneous self-assembly of cell suspensions in the absence of cell-adhesive substrates (e.g., inside agarose microwells). They hold great promise as a bioink for organ printing because they could potentially accelerate tissue formation and maturation [3, 16]. Notably, we have developed a robotic technology for rapid and scalable fabrication of a large number of tissue spheroids needed for organ printing [18].

To date, agarose molds have been extensively used to facilitate the assembly of tissue spheroids. The agarose molds can be fabricated by both direct (i.e., 3D printing) and indirect (i.e., casting) methods. In the case of indirect mold fabrication, the current technology typically involves microfabrication, including 3D printing, of the master mold (e.g., wax mold) for the subsequent agarose mold fabrication [19]. For direct mold fabrication, agarose has been printed into a mold to fabricate a small diameter vessel tissue engineering construct [17]. Here, we describe a proof-of-concept method to directly print a customized alginate mold for tissue fabrication. This has a distinct advantage in that printing alginate does not require low temperature plates for gelation nor heated dispenser units, as may be the case for printing agarose [17, 20, 21]. Similar to agarose, alginate is essentially a non-biodegradable, bio-inert, and biocompatible material. These are all highly desirable characteristics for printing a mold structure because it would maintain its shape fidelity to direct tissue morphology and not interact with the forming tissue. Also, it allows for the fabrication of customized molds for specific applications.

In this study, we proposed and developed a 3D mold-printing technology to produce biocompatible, bio-inert alginate hydrogel molds, which can facilitate the fusion process of tissue spheroids to form scaffold-free tissue-engineered constructs with defined 3D structures. Specifically, we have developed a 3D printing technology to print micro-droplets of alginate solution on calcium-containing substrates in a layer-by-layer manner to fabricate a variety of 3D structures. Further, we utilized this technology to fabricate ring-shaped 3D hydrogel molds for toroid-shaped tissue unit fabrication. Tissue spheroids composed of 50% endothelial cells and 50% smooth muscle cells were robotically placed into the 3D printed alginate molds, and they were found to rapidly fuse together into toroid-shaped tissue units. Histological and immunofluorescence analyses indicated the critical role of cell-secreted collagen I in tissue formation and maturation.

Materials and methods

Configuration of the Palmetto 3D bioprinter

The Palmetto 3D Printer (Supplementary Fig. 1A), is a fully automated 3D printer developed by the Medical University of South Carolina and Clemson University, and

assembled by Izumi International (Greenville, SC). The core devices for 3D printing include a three-axis motion control stage (Janome R2300N, Mahwah, NJ), a linear liquid dispensing system (Fishman, Hopkinton, MA) and a digital microscope (Dino Lite, Torrance, CA) to record the printing process. The printing hardware is housed in a sterile chamber, and the control and monitoring systems are set outside of the chamber. This 3D printer is capable of accurately dispensing micro-droplets of 1 μl volume per second at a resolution of 10 μm in all three (X, Y, and Z) dimensions. The system utilizes tapered free-flow tips with a range of 250-840 μm inner diameters (Fishman, Hopkinton, MA) as printing nozzles. In this application, 250 μm inner diameter tips were used as a printing nozzle for alginate and Pasteur pipettes (diameter ~1000 μm) were used to deposit tissue spheroids.

Alginate solution for 3D printing

3% sodium alginate solution (w/v) (FMC BioPolymer Co., Philadelphia, PA, USA) was selected as ink for 3D bioprinting because: 1) it can rapidly form hydrogels at the physiological condition by reacting with calcium ions and 2) it has suitable viscosity for robotic liquid dispensing, while maintaining the droplet shape after dispensing (i.e., a high contact angle). To rapidly crosslink micro-droplets of alginate solution into hydrogel, 100 mM $CaCl_2$ in 2% gelatin solution were utilized to prepare printing substrates according to the report of Brugger and coworkers [22].

Cell culture and spheroids fabrication

Human aortic smooth muscle cells (hSMCs) and human umbilical vein endothelial cells (HUVECs) (passage 3) were purchased from Lonza (Catalogue number: CC-2571 and C2517A respectively; Lonza, Basel, Switzerland). They were cultivated in media as suggested by the manufacturer (cell culture media: Lonza CC-3162 and CC-3182, respectively). At passage 5, the two cell types were mixed at a 1:1 ratio and then seeded into non-adhesive agarose hydrogels molds containing 35 concave recesses with hemispheric bottoms (400 μm diameter, 800 μm deep) to facilitate the formation of tissue cell spheroids.

The agarose hydrogel molds were prepared using commercial master micro-molds from Microtissues, Inc (Providence, RI) as negative replicates. 330 μL 1% sterile agarose solution was pipetted into the master micro-molds to form an agarose hydrogel mold, which was then carefully detached from the master mold and transferred into one well of a 24 well tissue culture plate.

The schematic presentation of cell spheroids fabrication is shown in the Supplementary Fig. 2. 3M hSMCs (Passage 5) and 3M HUVECs (Passage 5) were suspended in 2ml media composed of 50% hSMC media and 50% HUVEC media. 75 μl of the cell suspension was pipetted into each agarose mold. After the cells had settled down into the recesses of the mold (10 min), additional media was added (1.0ml/well for a 24 well plate) and exchanged as needed. In this way, 840 cell spheroids with diameter 300 μm can be routinely prepared using a 24 well plate containing 24 agarose hydrogel molds.

Histological and immunofluorescence analysis of tissue units

The printed tissue units were fixed for 30 minutes in 4% paraformaldehyde solution. After dehydration, tissues were processed for paraffin infiltration and embedding and sectioned. The paraffin sections were stained with hematoxylin–eosin and the images were captured using light microscope (Olympus BX40 equipped with a DP25 digital camera). For immunofluorescence staining, primary antibodies were rabbit anti-human collagen I (Cedarlane USA, Burlington, NC), mouse anti human α-smooth muscle actin (Sigma Aldrich, St. Louis, MO), and secondary antibodies were Alexa Fluor 546 and Alexa Fluor 647 (Invitrogen, Carlsbad, CA). First, a heat-induced epitope retrieval step was performed by 5 minutes pressure-cooking of the deparaffinized sections in 1.6 L PBS and 15ml antigen unmasking solution (H-3300, Vector Laboratories, Burlingame, CA). The sections were then permeabilized in a 0.1% Triton X-100 in PBS for 15 min at ambient temperature. After washing in PBS (3×), the tissues were incubated in Background Buster (Innovex Biosciences, Richmond, CA) for 30 minutes at ambient temperature. After washing in PBS (3 × 5 min), sections were incubated with primary antibodies diluted in 1.0% BSA in PBSA (PBS + 0.01% sodium azide) overnight in refrigerator. After washing in PBS (3 × 5 min), tissues were incubated with coordinate secondary antibodies diluted in 1.0% BSA in PBSA for 1h at ambient temperature. After copious washing in PBS, nuclei were counterstained with DAPI (Molecular Probes/Invitrogen, Eugene, OR) diluted in PBSA for 15 min at ambient temperature. Following the final wash procedure, individual slides were mounted under cover glass using Fluoro-Gel (Electron Microscopy Sciences, Hatfield, PA). A TCS SP5 AOBS laser scanning confocal microscope (Leica Microsystems, Inc., Exton, PA) was used to obtain fluorescent images.

Results and discussion

Optimization of printing parameters and printing algorithm

Alginate has been extensively used in the 3D bioprinting because it can robustly form cell compatible hydrogels in physiological conditions [26-28]. Notably, native alginate is not adhesive for cells and is also not broken down enzymatically in mammals [29, 30]. These are all highly desirable characteristics as molding materials to facilitate tissue formation. As a bio-inert material, alginate does not compete with cell-cell adhesion and therefore promote fusion process of tissue spheroids. In addition, it has limited biodegradability and sufficient mechanical property for molding [31].

In this work, we have developed a technology to robotically deposit micro-droplets of alginate solution onto calcium-containing gelatin substrates to construct 3D hydrogels (Fig. 1) [22]. A substrate of 100 mM $CaCl_2$ in 2% gelatin solution were prepare to serve as a reservoir for calcium ion. A lower concentration of calcium ions in the gelatin solution can lead to slow gelation process and undefined shape of microdroplets. It is important to note that some cell types may be sensitive to the free calcium ion that slowly diffuses from the physically crosslinked alginate mold [32, 33]. However, auxiliary tests confirmed high viability (>90%) post-printing using Ca^{2+}-sensitive porcine chondrocytes with an atypical calcium concentration (100mM) (Supplementary Fig. 3) [31, 32]. By using a layer-by-layer

approach, we can fabricate hydrogels with a number of defined 3D structures. This has been attributed to the upward diffusion of calcium ion from the gelatin substrates (Fig. 1) [22].

To ensure a high consistency among the alginate hydrogel micro-droplet formed on calcium-containing substrates, we have optimized both concentration of alginate solution and the volume of each droplet. A 3% sodium alginate solution (w/v) was found suitable for 3D printing because 1) it can rapidly form hydrogel micro-droplets on the calcium ion-containing gelatin substrates, and 2) it has proper viscosity for robotic liquid dispensing while maintaining the droplet shape after dispensing. The dispensing volume for 3% (w/v) alginate solution was set as 1 μl in this study because a smaller volume (0.5 μl) can give rise to larger variation among printed droplets (Fig. 2). To prevent the coalescence of newly printed droplets with their neighbors (Fig. 3a), we developed a printing algorithm to ensure that no printed droplet lands next to an un-gelled droplet and the final printed product maintained a defined structure as designed (Fig. 3b) [22].

To prove the feasibility of 3D hydrogel printing, we designed and printed hydrogels with different 3D geometries (cube, square frame, and pyramid). Both the printing scheme and the printed alginate hydrogel structures are shown in Fig. 4. This demonstrates the 3D hydrogel printing we developed here can allow for a proof-of-concept for the fabrication of alginate hydrogels with defined 3D structures. To quantify the printing accuracy, we measured the dimensions of a 3D printed cube structure and compared them to the design. As shown in Figure 4d, the cube structure was designed to have dimensions of 9.6 × 9.6 × 1.75 mm (X, Y, Z), which is a result of a printing design with dimensions of 9 mm × 9 mm (based on the center of dot) and a Z dimension defined by 5 layers. Typically, the first layer of alginate, which is printed onto the gelatin surface, has a height of ~0.7-0.8 mm, while the second and above layers of alginate, which is printed onto alginate surface, have heights of ~0.2-0.3 mm. The actual printed cube structure has dimensions of 9.6 × 9.8 × 1.8 mm, and it thus can be defined as an accurate printed structure [36]. Using the cube structure as a model, overnight culture in PBS resulted in an average increase in dimension (X, Y) of 1.8%, thus maintaining the designed parameters. This demonstrates the 3D hydrogel printing we developed here can allow for a proof-of-concept for the fabrication of alginate hydrogels with defined 3D structures. Given the quickly advancing field in biofabrication, improved parameters and limitations to bioprinting must be further optimized to achieve the highest needed control.

3D Printing alginate molds and robotically seeded spheroids

To utilize the 3D printed alginate hydrogel molds to facilitate fusion processes of tissue spheroids, we have designed ring-shaped alginate molds to fabricate toroid-shaped tissue units, which can be utilized to produce tissue engineering constructs (Fig 5) [37]. To prepare the mold, 24 layers of alginate hydrogel was printed in a layer-by-layer fashion to generate ring-shaped molds with inner diameter 5 mm, outer diameter 7 mm and height 3 mm over a time span of approximately 30 min (~30 secs/layer with ~1 min gelation time between layers). Subsequently, 840 spheroids (average diameter ~300 m) composed of 50% hSMCs and 50% HUVECs was robotically seeded into the mold to achieve a connected tissue [38,

39]. Tissue spheroids were selected as bioink for 3D bioprinting in this study because they have the potential to accelerate tissue formation and maturation [3, 16].

To utilize the Palmetto 3D Printer to robotically seed the cell spheroids, a variety of dispensing nozzles have been examined. Interestingly, Pasteur pipettes have been found most suitable for robotic dispensing of cell spheroid due to the smooth transition from upper portion of the pipette to the tip of the pipette (i.e., dispensing nozzle) and the diameter of pipette tip (~1000 μm) (Fig. 6). Customized Pasteur pipettes with a smaller tip diameter (~750 μm) were found difficult to seed cell spheroids since spheroids often blocked the dispensing nozzle.

Fabrication of toroid-shaped tissue units

After seeding into ring-shaped molds, the construct was moved to an incubator for 15 min to melt the calcium-containing gelatin. The melted gelatin solution was immediately replaced with fresh cell culture media to minimize exposure to high calcium concentration environment. The cell spheroids quickly began fusing into toroid-shaped tissue units after 3 days culture in a reliable manner, which is in agreement with previous research [16, 17]. Notably, the quality of the 3D printed mold can effectively affect the shape of the formed tissue units. These tissue units were cultivated for an additional 13 days to facilitate their maturation. To examine the fusion and maturation process, histological and immunofluorescence analysis were conducted. At day 4, the boundaries of many individual spheroids were clearly visible (Fig. 7a, 7b, 7j, and 7k) with many open spaces between spheroids (white arrow in Fig 7k). Notably, collagen I was often found between the boundaries of two adjacent spheroids (Fig. 7k and 7l). As a structural ECM protein with cell adhesion motifs (e.g., RGD peptide sequence), collagen I was thought to function as adhesive to facilitate the fusion process of the spheroids. At day 8, most spheroids were found to be closely associated to each other, while gaps between some spheroids were still found (white arrows in Fig. 7d and 7e). At day 16, the spheroids had fused into a complete tissue with abundant, newly synthesized collagen I (Fig. 7m). In addition, the collage I had filled all the gaps between spheroids (white arrows in Fig. 7o). This data indicates collagen I plays a critical role in promoting cell-cell adhesion, tissue formation and maturation. This is consistent with the previous report that cell-adhesive ECM proteins can crosslink adjacent cells together by binding to their cell surface receptor (e.g., integrin) and promote tissue cohesion [40]. In addition, the day 16-tissue units were stained for smooth muscle cells and endothelial cells (Fig 7p-r). The high expression of specific molecular markers for both cell types (i.e., smooth muscle actin and VWF) indicates high cell viability and normal cell behavior after 16-day cell culture.

Conclusion

3D printing holds great promise for rapid, scalable fabrication of tissue engineering constructs. Here, we have developed a robust technology to robotically 3D print alginate hydrogel molds to facilitate fusion process of tissue-cell spheroids for the fabrication of scaffold-free tissue units. To this end, we have optimized both printing parameters and printing algorithm for constructions of alginate hydrogels with defined 3D architectures. In

addition, we also utilized the Palmetto 3D Printer to robotically place tissues spheroids into the alginate molds to rapidly fuse into toroid-shaped tissue units. Our system has displayed the proof-of-concept for using alginate as a 3D printable, molding material to facilitate scaffold-free tissue unit fabrication. The approach developed in this manuscript could be used to fabricate various open-structured molds (e.g., honeycomb-shaped molds) for the construction of complex structures [19]. Further calibrations and improvements to the system are needed for the fabrication of non-open-structured molds to prepare tissues with more complex shapes, such as small diameter blood vessels, which require printing spheroids and alginate in a more controlled manner. Given the rapid development in printing technology, we expect that the technology developed here can be used to fabricate tissues with complex structures for tissue engineering and drug testing applications.

Supplementary Material

Refer to Web version on PubMed Central for supplementary material.

Acknowledgement

The work is supported by the National Science Foundation (NSF - EPS-0903795), the startup funds from Clemson University, and the National Institutes of Health (8P20 GM103444). This study used the services of the Morphology, Imaging and Instrumentation Core, which is supported by NIH-NIGMS P30 GM103342 to the South Carolina COBRE for Developmentally Based Cardiovascular Diseases. We would like to thank Agnes Nagy Mehesz and Sandra Klatt for the support in cell culture, spheroid fabrication and immunofluorescence staining.

Reference

[1]. Derby B. Printing and prototyping of tissues and scaffolds. Science. 2012; 338:921–6. [PubMed: 23161993]

[2]. Tasoglu S, Demirci U. Bioprinting for stem cell research. Trends in biotechnology. 2013; 31:10–9. [PubMed: 23260439]

[3]. Mironov V, Kasyanov V, Markwald RR. Organ printing: from bioprinter to organ biofabrication line. Current opinion in biotechnology. 2011; 22:667–73. [PubMed: 21419621]

[4]. Jakab K, Norotte C, Marga F, Murphy K, Vunjak-Novakovic G, Forgacs G. Tissue engineering by self-assembly and bio-printing of living cells. Biofabrication. 2010; 2:022001. [PubMed: 20811127]

[5]. Miller JS, Stevens KR, Yang MT, Baker BM, Nguyen DH, Cohen DM, et al. Rapid casting of patterned vascular networks for perfusable engineered three-dimensional tissues. Nature materials. 2012; 11:768–74.

[6]. Boland T, Mironov V, Gutowska A, Roth EA, Markwald RR. Cell and organ printing 2: fusion of cell aggregates in three-dimensional gels. The anatomical record Part A, Discoveries in molecular, cellular, and evolutionary biology. 2003; 272:497–502.

[7]. Mironov V, Boland T, Trusk T, Forgacs G, Markwald RR. Organ printing: computer-aided jet-based 3D tissue engineering. Trends in biotechnology. 2003; 21:157–61. [PubMed: 12679063]

[8]. Desroches BR, Zhang P, Choi BR, King ME, Maldonado AE, Li W, Rago A, Liu G, Nath N, Hartmann KM, Yang B, Koren G, Morgan JR, Mende U. Functional scaffold-free 3-D cardiac microtissues: a novel model for the investigation of heart cells. Am J Physiol Heart Circ Physiol. 2012; 302:H2031–42. [PubMed: 22427522]

[9]. Lee M, Wu BM, Dunn JCY. Effect of scaffold architecture and pore size on smooth muscle cell growth. J Biomed Mater Res A. 2008; 87:1010–6. [PubMed: 18257081]

[10]. Wang L, Shansky J, Borselli C, Mooney D, Vandenburgh H. Design and fabrication of a biodegradable, covalently crosslinked shape-memory alginate scaffold for cell and growth factor delivery. Tissue Eng Part A. 2012; 18:2000–7. [PubMed: 22646518]

[11]. Napolitano A, Dean D, Man A, Youssef J, Ho D, Rago A, Lech M, Morgan J. Scaffold-free three-dimensional cell culture utilizing micromolded nonadhesive hydrogels. Biotechniques. 2007; 43:494–500. [PubMed: 18019341]

[12]. Stevens KR, Pabon L, Muskheli V, Murry CE. Scaffold-Free Human Cardiac Tissue Patch Created from Embryonic Stem Cells. Tissue Eng Part A. 2009; 15:1211–22. [PubMed: 19063661]

[13]. Pok S, Myers JD, Madihally SV, Jacot JG. A multilayered scaffold of a chitosan and gelatin hydrogel supported by a PCL core for cardiac tissue engineering. Acta Biomater. 2013; 9:5630–42. [PubMed: 23128158]

[14]. Hollister SJ. Porous scaffold design for tissue engineering. Nature materials. 2005; 4:518–24.

[15]. Langer R, Vacanti JP. Tissue engineering. Science. 1993; 260:920–6. [PubMed: 8493529]

[16]. Mironov V, Visconti RP, Kasyanov V, Forgacs G, Drake CJ, Markwald RR. Organ printing: tissue spheroids as building blocks. Biomaterials. 2009; 30:2164–74. [PubMed: 19176247]

[17]. Norotte C, Marga FS, Niklason LE, Forgacs G. Scaffold-free vascular tissue engineering using bioprinting. Biomaterials. 2009; 30:5910–7. [PubMed: 19664819]

[18]. Mehesz AN, Brown J, Hajdu Z, Beaver W, da Silva JV, Visconti RP, et al. Scalable robotic biofabrication of tissue spheroids. Biofabrication. 2011; 3:025002. [PubMed: 21562365]

[19]. Dean DM, Napolitano AP, Youssef J, Morgan JR. Rods, tori, and honeycombs: the directed self-assembly of microtissues with prescribed microscale geometries. FASEB J. 2008; 21:4005–4012. [PubMed: 17627028]

[20]. Lee W, Lee V, Polio S, Keegan P, Lee JH, Fischer K, et al. On-demand three-dimensional freeform fabrication of multi-layered hydrogel scaffold with fluidic channels. Biotechnology and bioengineering. 2010; 105:1178–86. [PubMed: 19953677]

[21]. Billiet T, Gevaert E, De Schryver T, Cornelissen M, Dubruel P. The 3D printing of gelatin methacrylamide cell-laden tissue-engineered constructs with high cell viability. Biomaterials. 2014; 35:49–62. [PubMed: 24112804]

[22]. Pataky K, Braschler T, Negro A, Renaud P, Lutolf MP, Brugger J. Microdrop Printing of Hydrogel Bioinks into 3D Tissue-Like Geometries. Adv Mater. 2011

[23]. Xu C, Chai W, Huang Y, Markwald RR. Scaffold-free inkjet printing of three-dimensional zigzag cellular tubes. Biotechnology and bioengineering. 2012; 109:3152–60. [PubMed: 22767299]

[24]. Shim J-H, Lee J-S, Kim JY, Cho D-W. Bioprinting of a mechanically enhanced three-dimensional dual cell-laden construct for osteochondral tissue engineering using a multi-head tissue/organ building system. J Micromechanics Microengineering. 2012; 22:085014.

[25]. Rowley JA, Madlambayan G, Mooney DJ. Alginate hydrogels as synthetic extracellular matrix materials. Biomaterials. 1999; 20:45–53. [PubMed: 9916770]

[26]. Hunt NC, Shelton RM, Henderson DJ, Grover LM. Calcium-alginate hydrogel-encapsulated fibroblasts provide sustained release of vascular endothelial growth factor. Tissue engineering Part A. 2013; 19:905–14. [PubMed: 23082964]

[27]. Hunt NC, Shelton RM, Grover LM. Reversible mitotic and metabolic inhibition following the encapsulation of fibroblasts in alginate hydrogels. Biomaterials. 2009; 30:6435–43. [PubMed: 19709739]

[28]. Orive G, Carcaboso AM, Hernandez RM, Gascon AR, Pedraz JL. Biocompatibility evaluation of different alginates and alginate-based microcapsules. Biomacromolecules. 2005; 6:927–31. [PubMed: 15762661]

[29]. Lansdown AB, Payne MJ. An evaluation of the local reaction and biodegradation of calcium sodium alginate (Kaltostat) following subcutaneous implantation in the rat. Journal of the Royal College of Surgeons of Edinburgh. 1994; 39:284–8. [PubMed: 7861335]

[30]. Smetana K Jr. Cell biology of hydrogels. Biomaterials. 1993; 14:1046–50. [PubMed: 8312457]

[31]. Augst AD, Kong HJ, Mooney DJ. Alginate hydrogels as biomaterials. Macromolecular bioscience. 2006; 6:623–33. [PubMed: 16881042]

[32]. Kuo CK, Ma PX. Ionically crosslinked alginate hydrogels as scaffolds for tissue engineering: part 1. Structure, gelation rate and mechanical properties. Biomaterials. 2001; 22:511–21. [PubMed: 11219714]

[33]. Ugwu A, Smith GL, Miller DJ, McGrath J. Calcium-sensitivity of smooth muscle contraction in the isolated perfused rat tail artery. African J Biomed Res. 2002; 5:33–42.

[34]. Yellowley CE, Hancox JC, Donahue HJ. Effects of cell swelling on intracellular calcium and membrane currents in bovine articular chondrocytes. Journal of cellular biochemistry. 2002; 86:290–301. [PubMed: 12111998]

[35]. Raizman I, De Croos JN, Pilliar R, Kandel RA. Calcium regulates cyclic compression-induced early changes in chondrocytes during in vitro cartilage tissue formation. Cell calcium. 2010; 48:232–42. [PubMed: 20932575]

[36]. Kang KH, Hockaday LA, Butcher JT. Quantitative optimization of solid freeform deposition of aqueous hydrogels. Biofabrication. 2013; 5:035001. [PubMed: 23636927]

[37]. Livoti CM, Morgan JR. Self-assembly and tissue fusion of toroid-shaped minimal building units. Tissue engineering Part A. 2010; 16:2051–61. [PubMed: 20109063]

[38]. Fleming PA, Argraves WS, Gentile C, Neagu A, Forgacs G, Drake CJ. Fusion of uniluminal vascular spheroids: a model for assembly of blood vessels. Developmental dynamics: an official publication of the American Association of Anatomists. 2010; 239:398–406. [PubMed: 19918756]

[39]. Gentile C, Fleming PA, Mironov V, Argraves KM, Argraves WS, Drake CJ. VEGF-mediated fusion in the generation of uniluminal vascular spheroids. Developmental dynamics: an official publication of the American Association of Anatomists. 2008; 237:2918–25. [PubMed: 18816835]

[40]. Robinson EE, Zazzali KM, Corbett SA, Foty RA. Alpha5beta1 integrin mediates strong tissue cohesion. Journal of cell science. 2003; 116:377–86. [PubMed: 12482923]

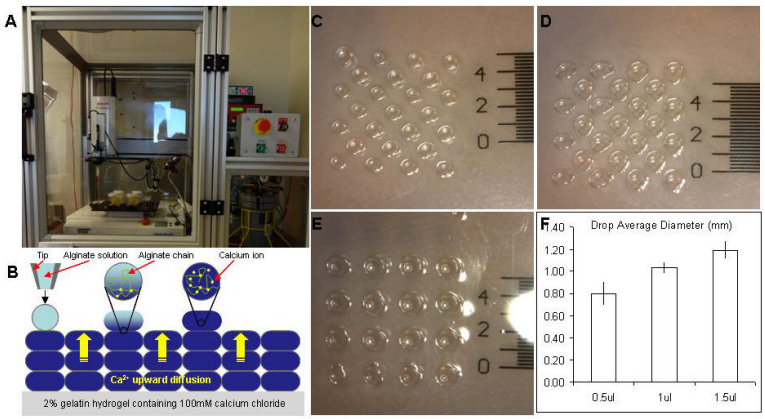

Figure 1.

Schematic presentation of 3D alginate hydrogel printing on calcium-containing gelatin substrate. Adapted from the reference 19.

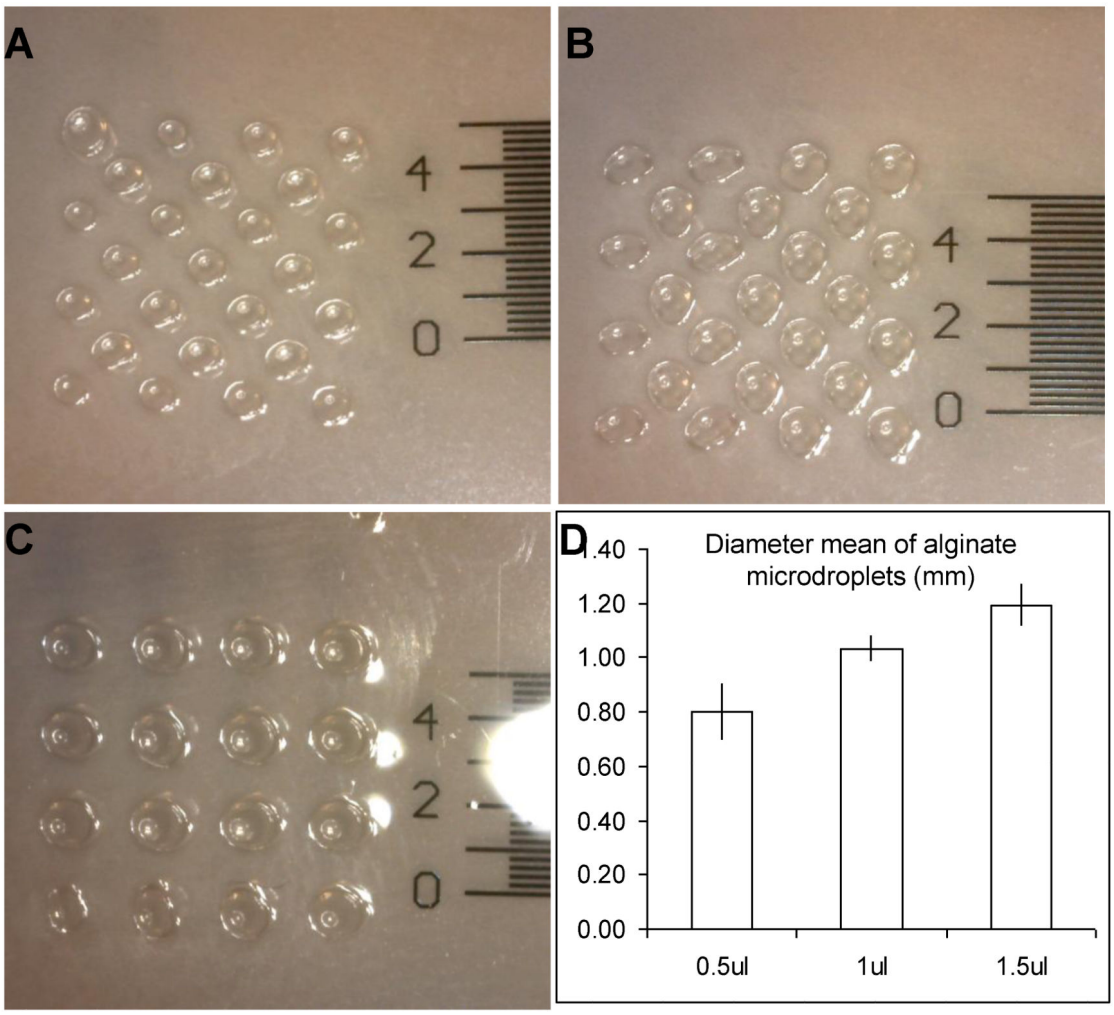

Figure 2.

The size of alginate microdroplets (A=0.5, B=1.0, and C=1.5μl) printed on calcium containing gelatin substrates.

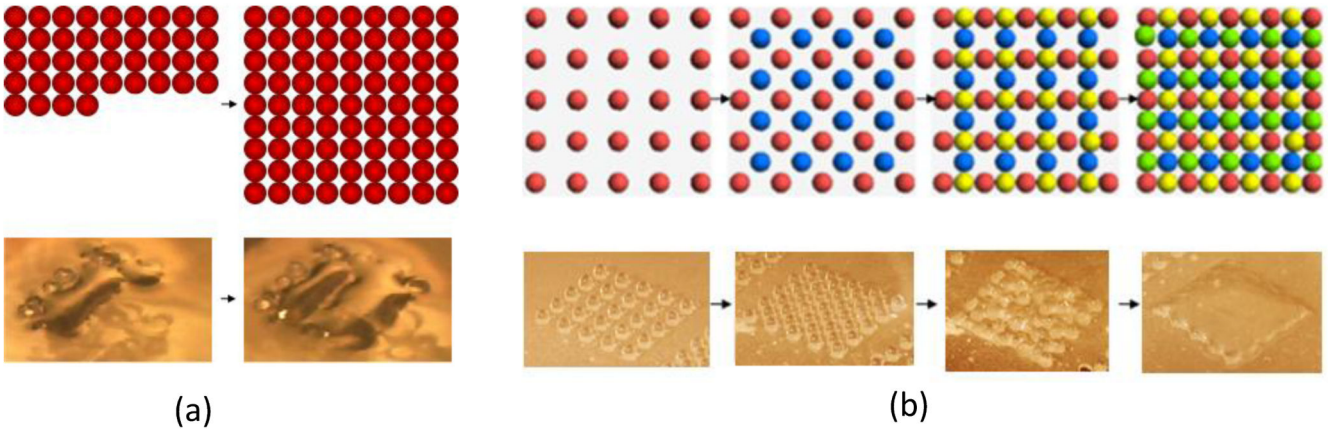

Figure 3.

(a) Printing algorithm before optimization: printing microdroplets of alginate solution next to each other can lead to the coalescence of newly printed droplets. (b) Printing algorithm after optimization: printing microdroplets of alginate solution in 4 steps to to ensure that no printed droplet lands next to an un-gelled droplet and the final printed product can maintain a defined structure as designed.

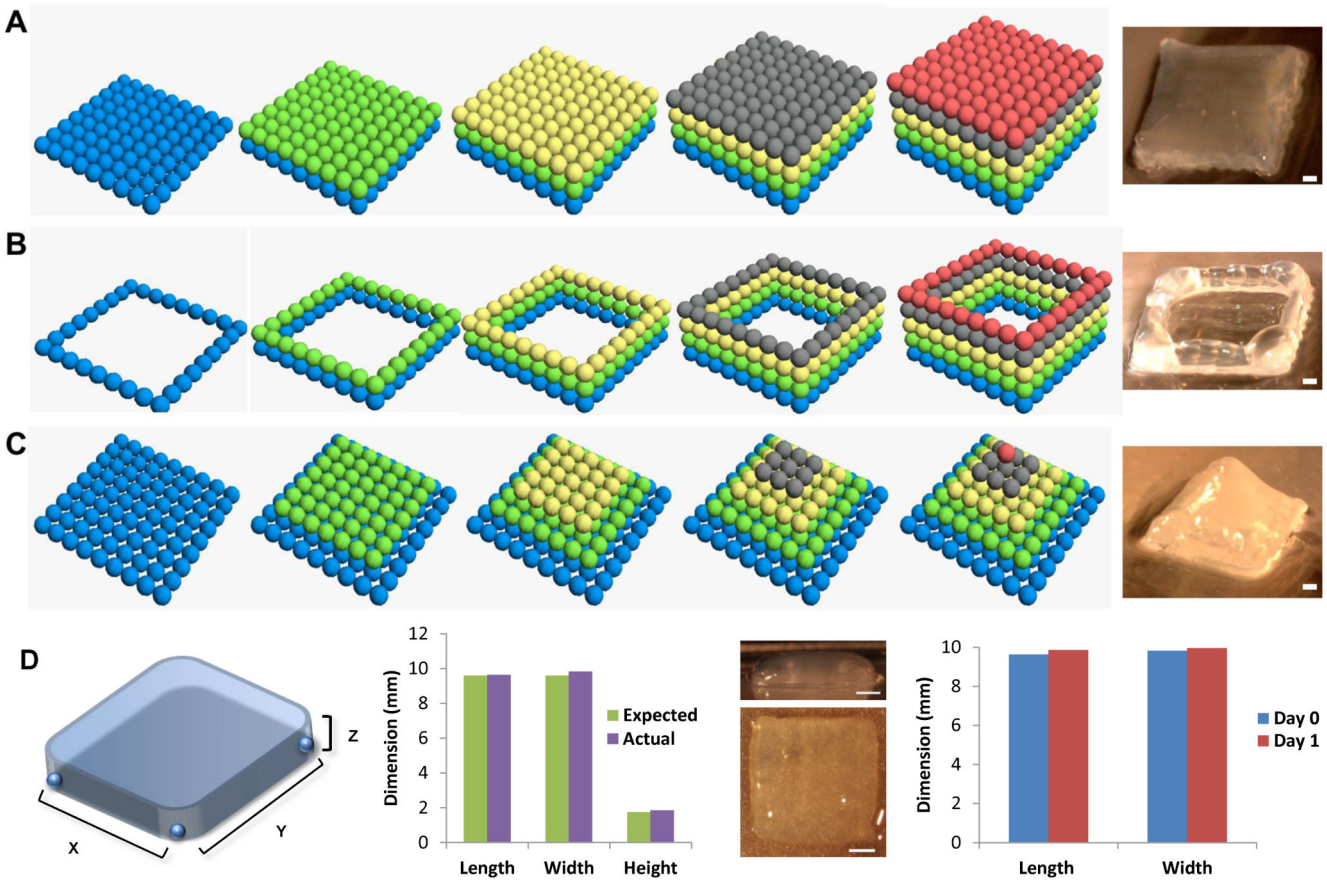

Figure 4.

Microdroplets facilitated 3D printing alginate hydrogels with different geometries (cube (a), square frame (b) and pyramid (c)).: the left is the schematic presentation of 3D printing algorithm used to print 3D structures shown in the right. Each layer was printed using an multi-step algorithm similar to the one shown in Figure 3. The optimal expected dimensions of 9.6 × 9.6 × 1.75 mm were based on a design of 9 mm × 9 mm in the X and Y dimension (measured from the dot center) and a Z dimension defined by 5 layers (d). The scale bar for (a),(b), and (c) is 1 mm. The scale bar for (d) is 2 mm. The blue, green, yellow, grey and red represent the 1st, 2nd, 3rd, 4th, and 5th layer of bioprinted alginate microdroplets, respectively.

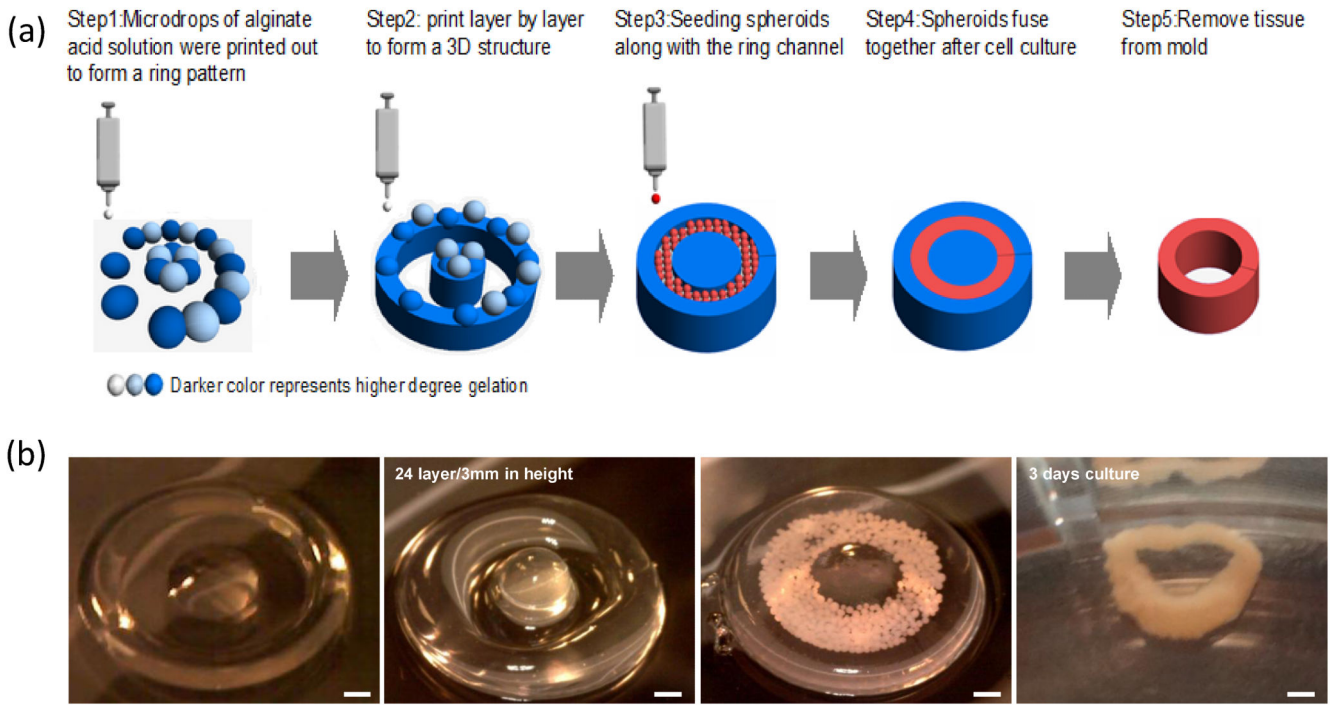

Figure 5.

Schematic presentation (a) and actual product (b) of 3D alginate hydrogel printing for tissue unit fabrication using vascular spheroids (i.e., containing smooth muscle cells and endothelial cells). Scale bar is 1mm

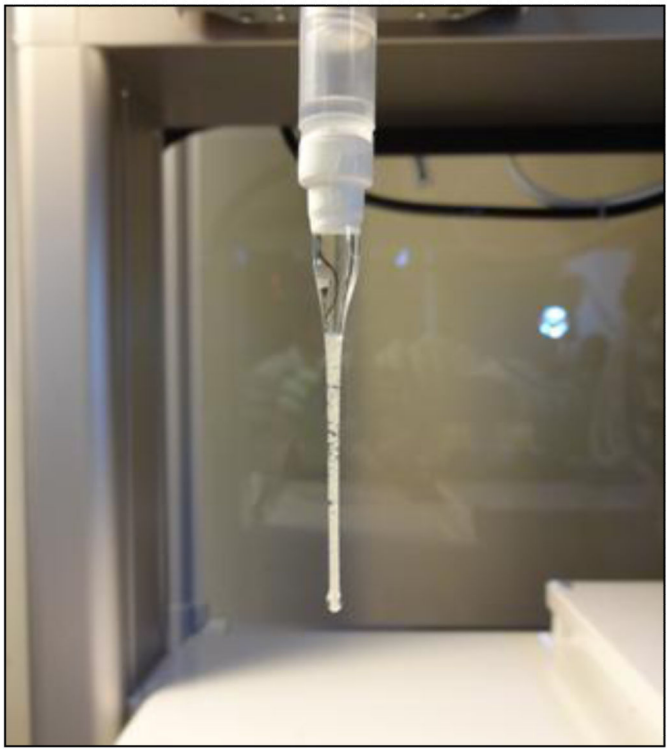

Figure 6.
A picture showing the pasture pipette printing tip loaded with tissue spheroids for dispensing.

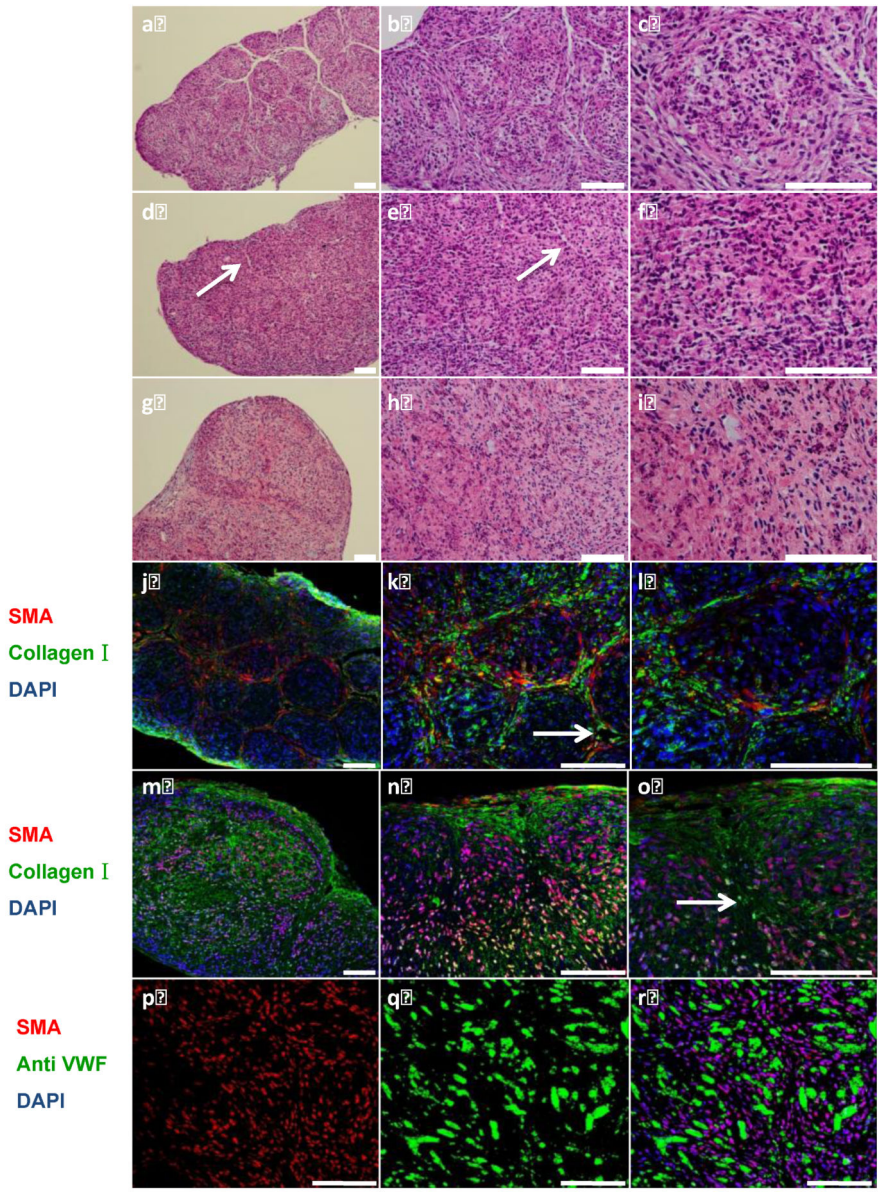

Figure 7.

Histological and immunofluorescence analysis of the tissue units cultured for 4, 8 and 16 days. (a,b,c) H&E staining for tissue units cultured for 4 days at 10×, 20× and 40× magnification, respectively. (d,e,f) H&E staining for tissue units cultured for 8 days at 10×, 20× and 40× magnification, respectively. (g,h,i) H&E staining for tissue units cultured for 16 days at 10×, 20× and 40× magnification, respectively. (j,k,l) immunofluorescence analysis of tissue units cultured for 4 days at 20×, 40× and 63 × magnification. (m,n,o) immunofluorescence analysis of tissue units cultured for 16 days at 20×, 40× and 63 × magnification. (p,q,r) immunofluorescence analysis of tissue units cultured for 16 days at 40× magnification for smooth muscle actin, anti VWF and merge picture. Scale bar is 100μm